Lawrence Berkeley National Laboratory

Recent Work

Title

Ligand removal of Au_{25} nanoclusters by thermal and electrochemical treatments for selective CO_2 electroreduction to CO.

Permalink

https://escholarship.org/uc/item/6w1300zj

Journal

The Journal of chemical physics, 155(5)

ISSN

0021-9606

Authors

Chen, Shouping
Li, Mufan
Yu, Sunmoon
et al.

Publication Date

2021-08-01

DOI

10.1063/5.0059363

Peer reviewed

eScholarship.org Powered by the California Digital Library
University of California

Ligand removal of Au25 nanoclusters by thermal and electrochemical treatments for selective CO2 electroreduction to CO

Shouping Chen, Mufan Li, Sunmoon Yu, Sheena Louisia, Wesley Chuang, Mengyu Gao, Chubai Chen, Jianbo Jin, Miquel B. Salmeron, Peidong Yang, et al.
Department of Materials Science and Engineering, University of California, Berkeley, California 94720, USA
2Chemical Sciences Division, Lawrence Berkeley National Laboratory, Berkeley, California 94720, USA
3Department of Chemistry, University of California, Berkeley, California 94720, USA 4Kavli Energy NanoScience Institute, Berkeley, California 94720, USA Note: This paper is part of the JCP Special Topic on From Atom-Precise Nanoclusters

ABSTRACT Undercoordinated metal nanoclusters have shown great promise for various catalytic applications. However, their activity is often limited by the covalently bonded ligands, which could block the active surface sites. Here, we investigate the ligand removal process for Au25 nanoclusters using both thermal and electrochemical treatments, as well as its impact on the electroreduction of CO2 to CO. The Au25 nanoclusters are synthesized with 2-phenylethanethiol as the capping agent and anchored on sulfur-doped graphene. The thiolate ligands can be readily removed under either thermal annealing at ≥ 180 ○C or electrochemical biasing at ≤ −0.5 V vs reversible hydrogen electrode, as evidenced by the Cu underpotential deposition surface area measurement, x-ray photoelectron spectroscopy, and extended x-ray absorption fine structure spectroscopy. However, these ligand-removing treatments also trigger the structural evolution of Au25 nanoclusters concomitantly. The thermally and electrochemically treated Au25 nanoclusters show enhanced activity and selectivity for the electrochemical CO2-to-CO conversion than their pristine counterpart, which is attributed to the exposure of undercoordinated Au sites on the surface after ligand removal. This work provides facile s

INTRODUCTION Metal nanoclusters with atomically precise structures are promising candidates for a wide range of catalytic reactions, among which CO2 reduction has drawn growing attention as a sustainable approach to producing value-added fuels and chemicals.1–4 These sub-2 nm clusters are typically synthesized with metal atoms as the core and thiolate ligands as the shell, which together form a well-defined motif to control the cluster size and crystal structure.5–7 Due to their ultrasmall size, the nanoclusters develop quantized electronic structures and possess low coordination numbers of metal atoms.8,9 These unique features provide the nanoclusters with superior catalytic properties, as compared with the larger nanoparticles.10 For example, multiple ultrafine clusters have shown remarkable catalytic performances for electrochemical CO2 reduction, in which undercoordinated surface sites have been identified as the true active centers to improve the reactivity.11–13 Therefore, it is critical to preserve and expose the undercoordination of metal nanoclusters as much as possible to further promote CO2 electrocatalysis. The stability problem always remains a great challenge for exploring the catalytic behaviors of metal nanoclusters.14 They tend to agglomerate into larger nanoparticles under harsh reaction conditions, which considerably destroys the nature of their undercoordination.15 To tackle this issue, sulfur-doped graphene (S-G) has been employed to stabilize the nanoclusters through strong catalyst–support interaction, which inhibits significant cluster coalescence within electrocatalytic environments.16 Although the stability is enhanced, the activity of metal nanoclusters is still limited by the protecting thiolate ligands on the surface.17 For example, thiols can passivate the surface of Au catalysts because of the strong Au–S bonding.18,19 Despite the possibility of changing the electronic structure of metal clusters, these capping ligands not only impose steric restriction on the accessibility of molecular reactants but also block the active undercoordinated surface atoms from being available for catalysis.20,21 Furthermore, theoretical calculations have predicted that the ligand-removed sites on metal nanoclusters are responsible for enhanced CO2 reduction properties.22 In this regard, here we study the removal process of thiolate ligands from Au25 nanoclusters by both thermal annealing and electrochemical biasing. The Au25 nanoclusters after ligand-removing treatments exhibit improved activity and selectivity for CO2 electroreduction to CO.

RESULTS AND DISCUSSION Neutrally charged Au25 [Au25(PET)18, PET = 2-phenylethanethiol] nanoclusters were prepared following a reported solution-phase method and purified by passing through a silica column and a size-exclusion column subsequently (for experimental details, see the Methods section of the supplementary material).23 The successful synthesis of charge-neutral and pure Au25 nanoclusters was confirmed by the ultraviolet-visible spectroscopy (UV–vis) and electrospray ionization-mass spectrometry (ESI-MS). The UV–vis spectrum [Fig. 1(a)] shows characteristic absorption peaks at 401, 461, 639, and 693 nm, which are consistent with the previously published results for neutral Au25 nanoclusters.23 The ESI-MS spectrum [Fig. 1(b)] exhibits signature peaks only at 7393 and 3696 of m/z, which conforms to the molecular weight of Au25(PET)18 with atomic accuracy and excludes the existence of other impurities. The crystal structure of Au25 nanoclusters has been reported in the literature, which contains a Au13 icosahedron core surrounded by a shell of six –S–Au–S–Au–S– semiring motifs (Fig. S1).24 The transmission electron microscopy (TEM) image [Fig. 1(c)] shows the ultrasmall size and uniform distribution of Au25 nanoclusters at 1.3 ± 0.3 nm, which agrees well with the previously reported crystallography measurement.25 The Au25 nanoclusters were then loaded on S-G by stir-mixing in toluene at room temperature for 1 h to obtain Au25/S-G.16 The TEM image of Au25/S-G [Fig. 1(d)] demonstrates that the Au25 nanoclusters were evenly distributed on the S-G substrate without noticeable aggregation or sintering, which was attributed to the dopant-anchoring effect of S-G.16 The

aberration-corrected scanning transmission electron microscopy (STEM) image [Fig. 1(d)] also verifies the size of the Au25 nanocluster after loading on S-G, in which the bright dots represent the Au atoms. To investigate the ligand removal of Au25 nanoclusters, we first applied thermal treatment, which has been a general approach to strip away the ligands.17,21 The Au25/S-G with 57 μg of Au, as determined by the inductively coupled plasma-optical emission spectroscopy (ICP-OES), was annealed in a 10% H2/Ar atmosphere at different temperatures from 120 to 220 ○C. The surface-sensitive Cu underpotential deposition (UPD) measurement was utilized to evaluate the degree of ligand removal by determining the surface area of exposed or ligand-free Au.26 The electrochemically active surface area was calculated using the charges associated with the anodic stripping peak.27 Both pristine and 120 ○C annealed Au25/S-G showed no peaks in the Cu UPD curves with surface areas close to zero [Figs. 2(a) and 2(b)], which implied that their Au surfaces were inaccessible as they were fully blocked by the thiolate ligands. A weak stripping peak was observed when the annealing temperature reached 150 ○C, corresponding to a surface area of 1 cm2 (Fig. S2a). This indicates that the staple ligands of Au25 nanoclusters start to be cleaved at 150 ○C. The anodic peak became larger at 180 ○C, of which the surface area was 6 cm2 , and further grew at 220 ○C, of which the surface area was 9 cm2 [Figs. 2(a) and 2(b)]. This suggests that the capping ligands can be readily removed at elevated temperatures (≥ 180 ○C), leaving a large amount of Au exposed on the surface. The extent of ligand removal was further estimated by the surface-specific x-ray photoelectron spectroscopy (XPS) technique via probing the oxidation state of Au in Au25/S-G. The pristine and 120 ○C annealed Au25/S-G exhibited relatively higher binding energies for Au [Fig. 2(c)], which were in accord with higher oxidation states. This implies that their surface Au atoms are still covalently bonded to the S atoms of the thiolate ligands. As the temperature increased to 150, 180, and 220 ○C, the binding energies of Au in Au25/S-G gradually turned lower [Fig. 2(c) and Fig. S2b], suggesting that the surface Au became progressively more metallic. This indicates that more Au–S bonds are being cleaved, and thus, more thiolate ligands are removed at higher temperatures. Moreover, the ligand removal process was also studied by the extended x-ray absorption fine structure (EXAFS) spectroscopy at the Au L3- edge, which probed the coordination environments of Au atoms. The pristine Au25/S-G showed a similar spectrum to that reported in the literature [Fig. 2(d)], in which the peak at ∼1.9 Å corresponded to the Au–S coordination, and the following peaks at around 2.4 and 2.8 Å represented the Au–Au coordination.17 The high intensity of the Au–S peak for pristine Au25/S-G [Fig. 2(d)] indicates that the Au atoms are highly bonded to the S atoms. Then, as the annealing temperature increased to 180 and 220 ○C, the scattering amplitude of Au–S coordination gradually decreased [Fig. 2(d)], which suggested that a growing number of thiolate ligands were removed from the Au catalysts. All of Cu UPD, XPS, and EXAFS evidenced that thermal annealing could effectively strip away the surface ligands from Au25 nanoclusters. However, the thermal annealing also triggered the structural evolution simultaneously, as visualized by TEM. The Au25/S-G showed no obvious agglomeration at 120 ○C (Fig. S3a), at which the ligands were not removed at all. Once the ligands began to detach at 150 ○C, slight sintering intermittently appeared with the formation of low-density 2–4 nm nanoparticles (Fig. S3b). A noticeable number of larger nanoparticles, ranging from 4 to 8 nm, were observed when the ligands were largely removed at 180 ○C (Fig. S3c). In addition, subsequently, more nanoparticles of 4–8 nm were found, while more ligands were being removed at 220 ○C (Fig. S3d). The structural transformation was supported by EXAFS as well. The peak intensity of Au–Au coordination for pristine Au25/S-G was relatively small [Fig. 2(d)] owing to their ultrafine size. However, it became progressively larger at higher temperatures (180 and 220 ○C), as shown in Fig. 2(d), which correlated with the incremental appearance of larger particles seen in TEM (Fig. S3). These results suggest that the ligand removal from these nanoclusters without concomitant agglomeration remains to be a challenge. In addition to thermal treatment, next we further studied the ligand removal of Au25 nanoclusters by electrochemical treatment, which is another commonly used method to remove the capping ligands.28 The Au25/S-G, which contained 57 μg of Au measured by ICP, was biased in 0.1M KHCO3 under Ar purging at different potentials from −0.3 V vs reversible hydrogen electrode (VRHE) to −0.8 VRHE. The extent of ligand removal was also first examined by the Cu UPD test. After biasing at −0.3 VRHE, there was no distinct peak for Au25/S-G in the Cu UPD curve and its surface area was almost zero [Figs. 3(a) and 3(b)], indicating that this mild condition was insufficient to strip away the surface ligands. At −0.35 VRHE, a small desorption peak with a surface area of 1 cm2 showed up (Fig. S4a). Hence, we propose that −0.35 VRHE could be the critical point for ligand removal during the electrochemistry. Moreover, the Au25/S-G showed a non-negligible peak (surface area = 11 cm2) at −0.5 VRHE and exhibited an even more remarkable peak (surface area = 25 cm2) at −0.8 VRHE [Figs. 3(a) and 3(b)]. This implies that the protecting ligands can be removed significantly at negative potentials ≤ −0.5 VRHE, exposing abundant Au sites on the surface. It is worth mentioning that the surface areas under electrochemical biasing are overall larger than those under thermal annealing, which suggests that the electrochemical treatment is a more efficient tool to cleave the ligands from Au25 nanoclusters. Besides, the degree of ligand removal was studied by XPS as well. The Au surfaces of pristine and −0.3 VRHE biased Au25/S-G were both in higher oxidation states with higher binding energies [Fig. 3(c)], indicating that they were still largely covered by the thiolate ligands. Then, from −0.35 VRHE to −0.5 VRHE and further to −0.8 VRHE, the gradual Au 4f XPS peak shift to lower binding energy [Fig. 3(c) and Fig. S4b] suggested that more thiolate ligands got removed under more negative bias and the surface Au atoms became more metallic. Finally, the electrochemical ligand removal on Au25 clusters was also investigated by EXAFS. Figure 3(d) illustrates the lower intensity of Au–S coordination at more negative potentials (−0.5 VRHE and −0.8 VRHE), which proves that more protecting ligands are stripped away resulting from the application of bias. Although electrochemical treatment is a promising approach for the ligand removal of Au25 nanoclusters, similar to thermal treatment, it also induced a concurrent structural change. Cluster sintering was barely seen when the ligands still remained at −0.3 VRHE (Fig. S5a). At the starting point of ligand removal (−0.35 VRHE), the Au25/S-G exhibited a little agglomeration and formed a few nanoparticles of 2–4 nm (Fig. S5b).

When the ligands were more dominantly stripped away at −0.5 VRHE and −0.8 VRHE, more 2–4 nm nanoparticles were observed (Figs. S5c and S5d), which were apparently smaller than those found in thermal treatment (Figs. S3c and S3d). EXAFS was employed to confirm the structural evolution as well. As the applied potential reduced to −0.5 VRHE and −0.8 VRHE, the ramping amplitude of Au–Au coordination [Fig. 3(d)] suggested more cluster sintering, which was yet obviously smaller than that in thermal annealing [Fig. 2(d)]. These data collectively imply that the electrochemical treatment could more specifically cleave the Au–S bonds by applying reductive potentials, while the thermal treatment not only breaks the Au–S bonds but also increases the mobility of the entire cluster, leading to significant coalescence. Therefore, the electrochemical biasing is a more desirable way to remove the staple ligands without causing significant aggregation. Finally, we evaluated the impact of ligand removal on the catalytic properties of Au25 nanoclusters for CO2 electroreduction to CO. The Au25/S-G annealed at 150 ○C and that biased at −0.8 VRHE were utilized as thermally and electrochemically treated samples, respectively. The electrochemical CO2 reduction measurement was conducted in 0.1M KHCO3 solution under CO2 flow at a relatively low overpotential between −0.50 VRHE and −0.59 VRHE. For all the tests, CO and H2 were the only gas products detected by gas chromatography (GC), and a negligible amount of liquid product was found by proton nuclear magnetic resonance (1H NMR) spectroscopy (Fig. S6). Figure 4 shows that the Au25/S-G after thermal and electrochemical treatments demonstrated both higher faradaic efficiencies and larger partial current densities (normalized by Au mass loadings) for CO than the pristine catalyst. The CO faradaic efficiencies of thermally and electrochemically treated Au25/S-G at −0.59 VRHE were as high as 64% and 82%; however, it was only 49% for the pristine sample [Fig. 4(a)]. Meantime, the thermally and electrochemically treated Au25/S-G exhibited 2 and 7 times larger CO partial current densities than their pristine counterpart at −0.59 VRHE [Fig. 4(b)]. These results jointly suggest that the Au25/S-G after ligand removal showed both improved activity and enhanced selectivity for the electroreduction of CO2 to CO. The post-measurement characterizations reveal that although the Au25 nanoclusters did further evolve slightly after CO2 electrocatalysis (Fig. S7), the surface areas still followed the order of electrochemically treated Au25/S-G > thermally treated Au25/S-G > pristine Au25/S-G (Fig. S8), which was the same as the pre-reaction trend. Hence, we can conclude that the catalytic improvements of Au25/S-G after thermal and electrochemical treatments can be attributed to the exposure of undercoordinated Au sites on the surface after ligand removal, which favor the production of CO over H2. It is worth noting that the electrochemical biasing offered a better performance for CO2-to-CO electro-conversion than the thermal annealing (Fig. 4), which was again due to the higher surface area of exposed Au sites upon surface ligand removal (Fig. S8). Besides the active surface area, other properties, including coordination environment and electronic structure, may also affect the catalytic behavior of Au clusters, which needs further exploration.10,17 Finally, the Au25/S-G after different treatments also exhibited good stability over the course of long-term CO2 electrocatalysis (Fig. S9).

CONCLUSION In conclusion, we have successfully prepared pure Au25(PET)18 nanoclusters and anchored them on sulfur-doped graphene. The capping ligands could be significantly stripped away by both thermal annealing (≥ 180 ○C) and electrochemical biasing (≤ −0.5 VRHE). The degree of ligand removal was investigated by a combination of techniques including Cu UPD, XPS, and EXAFS. However, it was also noted that the aggressive thermal and electrochemical conditions inevitably induced the structural transformation of Au25 nanoclusters at the same time. The Au25 nanoclusters after ligand-removing treatments were both more active and more selective for CO2 electroreduction to CO than the pristine catalyst, which was contributed by the increased exposure of catalytically active surface Au sites associated with the removal of thiolate ligands. These findings could serve as a guideline on how to effectively remove the protecting ligands from undercoordinated metal nanoclusters to obtain superior catalytic properties.

SUPPLEMENTARY MATERIAL See the supplementary material for detailed experimental methods and additional characterization data, including structural models, Cu UPD curves, surface areas, XPS spectra, TEM images, and 1H NMR spectra.

ACKNOWLEDGMENTS This work was supported by the Director, Office of Science, Office of Basic Energy Sciences, Chemical Sciences, Geosciences, and Biosciences Division, of the US Department of Energy under Contract No. DE-AC02-05CH11231, FWP CH030201 (Catalysis Research Program). Aberration-corrected STEM and XPS were collected at the National Center for Electron Microscopy and the Imaging and Nanofabrication Facilities at the Molecular Foundry. The work at the Molecular Foundry was supported by the Director, Office of Science, Office of Basic Energy Sciences, of the U.S. Department of Energy under Contract No. DE-AC02- 05CH11231. The use of the Stanford Synchrotron Radiation Lightsource, SLAC National Accelerator Laboratory, was supported by the U.S. Department of Energy, Office of Science, Office of Basic Energy Sciences under Contract No. DE-AC02-76SF00515. We thank Simon Bare, Adam Hoffman, Matthew Latimer, and Erik Nelson for the collection and processing of the XAS data. We thank Z. Zhou and QB3-Berkeley's research facilities for assistance in obtaining ESI-MS data. We thank E. Kreimer of the Microanalytical Facility in the College of Chemistry, University of California at Berkeley, for access to ICP analysis. We thank H. Celik and acknowledge the University of California at Berkeley's NMR facility in the College of Chemistry for spectroscopic assistance. Instruments in the NMR facility in the

College of Chemistry are supported, in part, by the National Institutes of Health under Grant No. S10OD024998. S.Y. acknowledges support from the Samsung Fellowship. C.C. and J.J. acknowledge the fellowship from Suzhou Industrial Park.

REFERENCES 1H. Zhang, H. Liu, Z. Tian, D. Lu, Y. Yu, S. Cestellos-Blanco, K. K. Sakimoto, and P. Yang, Nat. Nanotechnol. 13, 900–905 (2018). 2Q. Tang, Y. Lee, D.-Y. Li, W. Choi, C. W. Liu, D. Lee, and D.-e. Jiang, J. Am. Chem. Soc. 139, 9728–9736 (2017). 3Y. Zhu, H. Qian, B. A. Drake, and R. Jin, Angew. Chem., Int. Ed. 49, 1295 (2010). 4M. B. Ross, P. De Luna, Y. Li, C.-T. Dinh, D. Kim, P. Yang, and E. H. Sargent, Nat. Catal. 2, 648–658 (2019). 5T. Ohta, M. Shibuta, H. Tsunoyama, Y. Negishi, T. Eguchi, and A. Nakajima, J. Phys. Chem. C 117, 3674–3679 (2013). 6X. Gao, S. He, C. Zhang, C. Du, X. Chen, W. Xing, S. Chen, A. Clayborne, and W. Chen, Adv. Sci. 3, 1600126 (2016). 7 I. Dolamic, S. Knoppe, A. Dass, and T. Burgi, Nat. Commun. 3, 798 (2012). 8R. Jin, Nanoscale 2, 343 (2010). 9 S. Yamazoe, S. Takano, W. Kurashige, T. Yokoyama, K. Nitta, Y. Negishi, and T. Tsukuda, Nat. Commun. 7, 10414 (2016). 10D. R. Kauffman, D. Alfonso, C. Matranga, H. Qian, and R. Jin, J. Am. Chem. Soc. 134, 10237 (2012). 11M. R. Narouz, K. M. Osten, P. J. Unsworth, R. W. Y. Man, K. Salorinne, S. Takano, R. Tomihara, S. Kaappa, S. Malola, C.-T. Dinh, J. D. Padmos, K. Ayoo, P. J. Garrett, M. Nambo, J. H. Horton, E. H. Sargent, H. Häkkinen, T. Tsukuda, and C. M. Crudden, Nat. Chem. 11, 419 (2019). 12B. Kim, H. Seong, J. T. Song, K. Kwak, H. Song, Y. C. Tan, G. Park, D. Lee, and J. Oh, ACS Energy Lett. 5, 749 (2020). 13Y. Li, D. Kim, S. Louisia, C. Xie, Q. Kong, S. Yu, T. Lin, S. Aloni, S. C. Fakra, and P. Yang, Proc. Natl. Acad. Sci. U. S. A. 117, 9194 (2020). 14B. Zhang, C. Chen, W. Chuang, S. Chen, and P. Yang, J. Am. Chem. Soc. 142, 11514 (2020). 15D. R. Kauffman, J. Thakkar, R. Siva, C. Matranga, P. R. Ohodnicki, C. Zeng, and R. Jin, ACS Appl. Mater. Interfaces 7, 15626 (2015). 16M. Li, B. Zhang, T. Cheng, S. Yu, S. Louisia, C. Chen, S. Chen, S. CestellosBlanco, W. A. Goddard, and P. Yang, "Sulfur-doped graphene anchoring of ultrafine Au25 nanoclusters for electrocatalysis," Nano Res. (published online) (2021). 17A. Shivhare, D. M. Chevrier, R. W. Purves, and R. W. J. Scott, J. Phys. Chem. C 117, 20007 (2013). 18H. Häkkinen, Nat. Chem. 4, 443 (2012). 19T. Bürgi, Nanoscale 7, 15553 (2015). 20J. Liu, K. S. Krishna, Y. B. Losovyj, S. Chattopadhyay, N. Lozova, J. T. Miller, J. J. Spivey, and C. S. S. R. Kumar, Chem. -Eur. J. 19, 10201 (2013). 21T. Yoskamtorn, S. Yamazoe, R. Takahata, J.-i. Nishigaki, A. Thivasasith, J. Limtrakul, and T. Tsukuda, ACS Catal. 4, 3696 (2014). 22N. Austin, S. Zhao, J. R. McKone, R. Jin, and G. Mpourmpakis, Catal. Sci. Technol. 8, 3795 (2018). 23S. Tian, L. Liao, J. Yuan, C. Yao, J. Chen, J. Yang, and Z. Wu, Chem. Commun. 52, 9873 (2016). 24M. Zhu, C. M. Aikens, F. J. Hollander, G. C. Schatz, and R. Jin, J. Am. Chem. Soc. 130, 5883 (2008). 25M. W. Heaven, A. Dass, P. S. White, K. M. Holt, and R. W. Murray, J. Am. Chem. Soc. 130, 3754 (2008).

FIG. 1. Structural characterizations of Au_{25} nanoclusters. (a) UV–vis spectrum; (b) ESI-MS spectrum, and (c) TEM image of Au_{25} nanoclusters. (d) TEM image of Au_{25} nanoclusters loaded on sulfur-doped graphene (Au_{25}/S-G). The inset is the aberration-corrected STEM image of the Au_{25} nanocluster after anchoring on S-G.

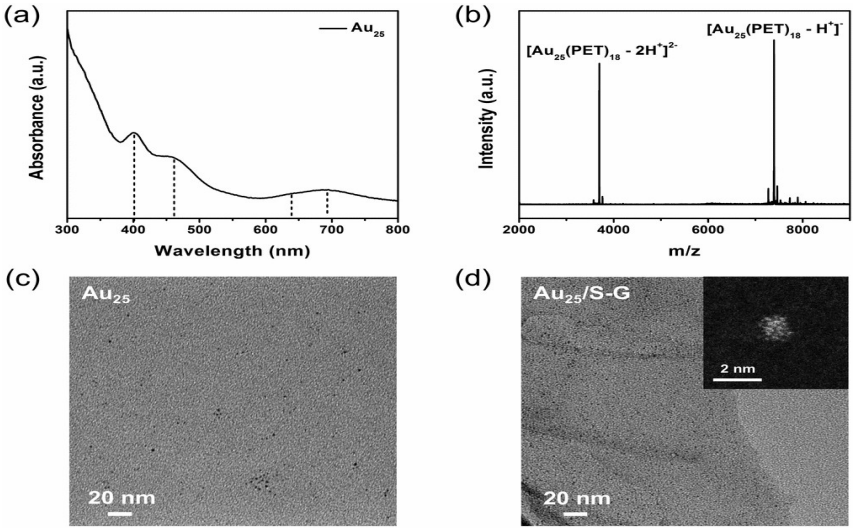

FIG. 2. Structural characterizations of Au_{25}/S-G after thermal treatments. (a) Cu UPD curves, (b) surface areas, (c) Au 4*f* XPS spectra, and (d) Au L_3-edge EXAFS spectra of Au_{25}/S-G annealed at different temperatures.

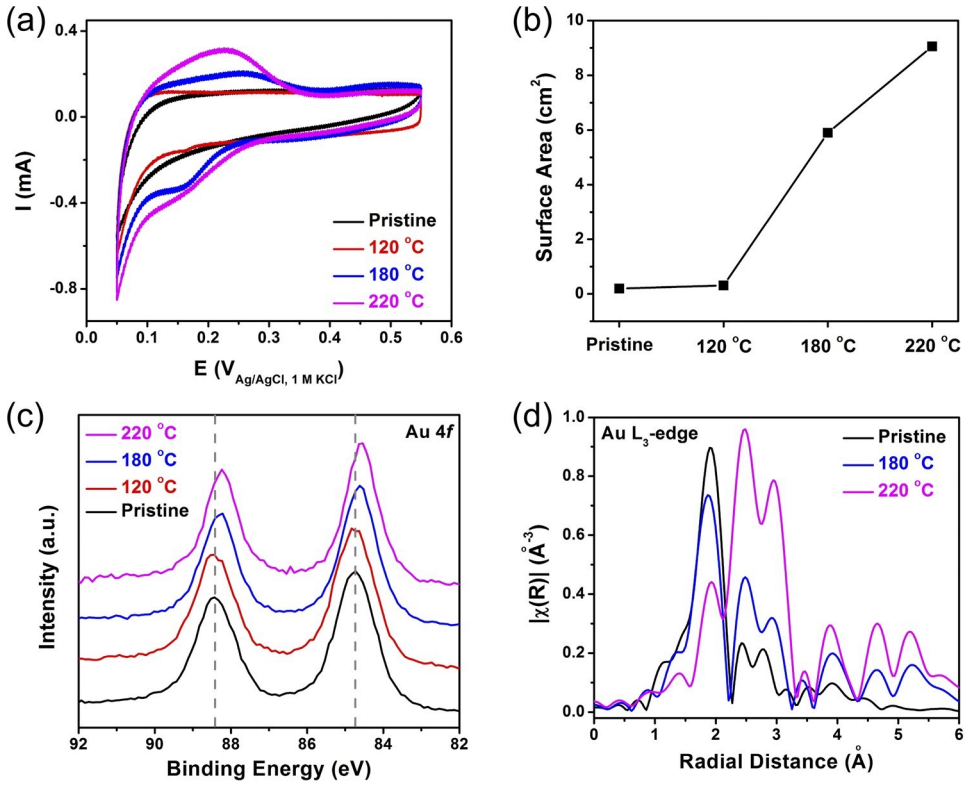

FIG. 3. Structural characterizations of Au_{25}/S-G after electrochemical treatments. (a) Cu UPD curves, (b) surface areas, (c) Au 4*f* XPS spectra, and (d) Au L_3-edge EXAFS spectra of Au_{25}/S-G biased at different potentials.

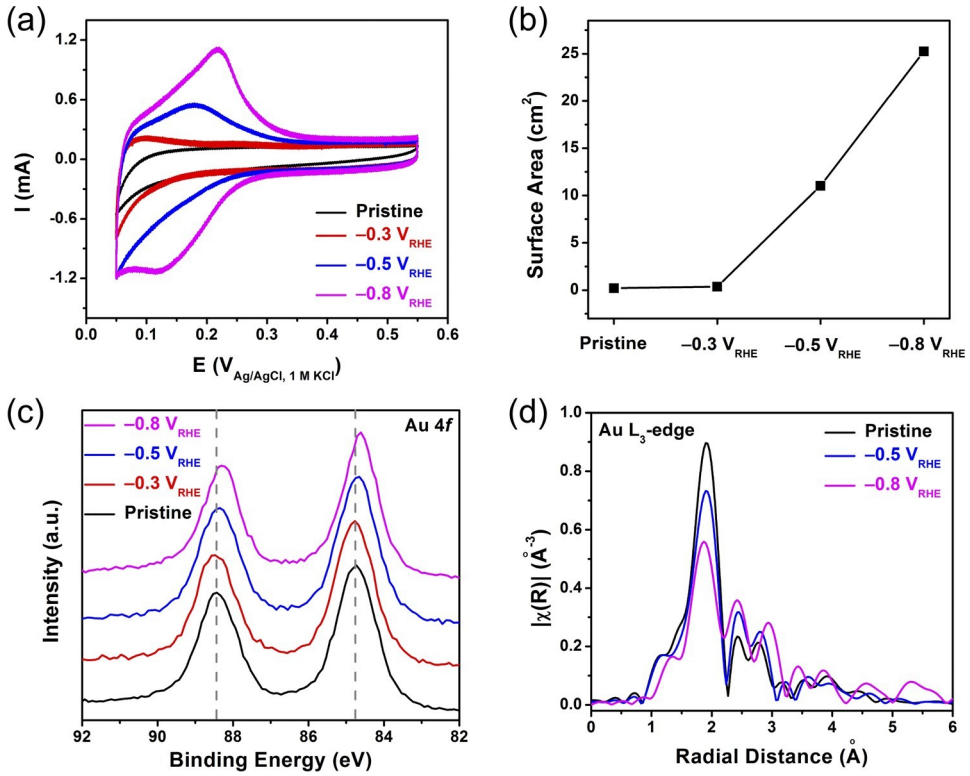

FIG. 4. CO_2 electrocatalytic properties of Au_{25}/S-G after different treatments. (a) Faradaic efficiencies (FEs) and (b) partial current densities (*j*, normalized by Au mass loadings) for CO of pristine, thermally treated, and electrochemically treated Au_{25}/S-G.